Journal of Catalysis **204,** 23–34 (2001)
doi:10.1006/jcat.2001.3360, available online at http://www.idealibrary.com on IDEAL®

Electrochemical Promotion and Metal–Support Interactions

J. Nicole,* D. Tsiplakides,† C. Pliangos,† X. E. Verykios,† Ch. Comninellis,* and C. G. Vayenas,†,[1]

*Department of Chemical Engineering, EPFL Lausanne, Switzerland; and †Department of Chemical Engineering, University of Patras, Patras, GR-26500, Greece

Received December 27, 2000; revised July 20, 2001; accepted July 20, 2001

Ethylene oxidation on IrO_2, which is a metal-type conducting metal oxide, and on Pt and Rh was used as a model reaction to compare the rate enhancement and kinetic modification induced by (i) electrochemical promotion (non-Faradic electrochemical modification of catalytic activity effect) via electrochemical O^{2-} supply from YSZ (Y_2O_3-stabilized ZrO_2) and TiO_2 and by (ii) metal–support interactions obtained by interfacing IrO_2 with TiO_2 (with and without electrochemical promotion) or by depositing dispersed Rh on TiO_2 and YSZ porous supports. It was found that the addition of TiO_2, which is catalytically inactive, to IrO_2 submicrometer particles enhances the activity of IrO_2 for C_2H_4 oxidation by a factor of 12 and that *the same* maximum rate enhancement is obtained via electrochemical promotion of the IrO_2 catalyst (i.e., via electrochemical O^{2-} supply to the IrO_2 catalyst from a YSZ solid electrolyte). Furthermore it was found that the IrO_2–TiO_2 catalyst mixtures can only be marginally promoted electrochemically. These observations show conclusively that the mechanism of metal (IrO_2)–support (TiO_2) interaction in the system IrO_2–TiO_2 is identical to that of the electrochemically promoted IrO_2–YSZ system (i.e., continuous O^{2-} supply to the IrO_2 catalyst surface). This conclusion is also corroborated by independent kinetic and XPS studies of electrochemical promotion of Pt utilizing TiO_2 (instead of YSZ) as the O^{2-} donor. The kinetics of C_2H_4 oxidation were investigated on Rh films interfaced with YSZ at various imposed potentials and thus imposed work function values, Φ (i.e., under conditions of electrochemical promotion and also on finely dispersed Rh catalysts deposited on various doped and undoped TiO_2 and YSZ porous supports of measured work function Φ). Again it was found that the reaction kinetics are affected in the same way upon varying the work function of the Rh film via electrical polarization of the Rh/YSZ interface or upon varying the work function of the support of the dispersed Rh catalysts. This observation confirms the equivalence of the promoting mechanism of metal–support interactions and electrochemical promotion (i.e., O^{2-} migration onto the catalyst surface). The results show conclusively that electrochemical promotion is an electrically controlled metal–support interaction and that at least certain types of metal–support interactions are induced by reverse spillover of oxygen anions from the carrier onto the surface of the metal crystallites.

INTRODUCTION

Metal–support interactions are known for years to play an important role in influencing the catalytic activity and selectivity of nanoscale metal crystallites constituting the active phase in commercial-supported catalysts (1–7). The nature of metal–support interactions has been the focal point of extensive research and dispute particularly after the discovery by Tauster *et al.* (8) of the phenomenon of strong metal–support interactions (SMSI). Although particle-size effects and electronic interactions between the metal particles and the support have been known for years to play a role, the SMSI effect was finally shown to be due to migration of ionic species from the support onto the catalyst particle surface ("decoration") (9).

Although SiO_2 and γ–Al_2O_3 are the most common high-surface-area industrial catalyst supports (considered in general to give rise to weak metal–support interactions), in recent years there has been an increasing tendency to replace these supports for numerous catalytic applications, mostly oxidations, with TiO_2- or ZrO_2-based porous supports (10). Little information exists in the open literature as to why this gradual substitution is taking place but it is a common understanding that these supports, generally believed to lead to stronger metal–support interactions, result in increased activity, selectivity, and useful lifetime of the metal particles deposited on them.

The purpose of the present communication is to compare:

(1) The catalytic rate enhancement of a model oxidation reaction induced on micro- or nanoparticles of two catalysts (IrO_2 and Rh) via classical metal–support interactions (i.e., via intimate contact with TiO_2 microparticles, or with highly porous TiO_2 and ZrO_2-based supports).

(2) The catalytic rate enhancement of the same model reaction induced by electrochemical promotion (11) of IrO_2 (12, 13) and Rh (14) porous catalyst films interfaced with YSZ, which is a pure O^{2-} conductor, and with TiO_2, which is a mixed O^{2-}–electronic (*n*-type) semiconductor. In the context of this comparison, the electrochemical promotion is also examined for catalyst films consisting of IrO_2–TiO_2 microparticle mixtures.

[1] To whom correspondence should be addressed. E-mail: cat@zeus.chemeng.upatras.gr.

0021-9517/01 $35.00

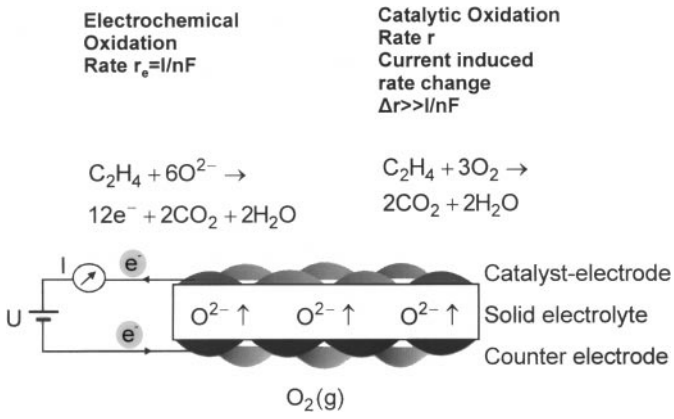

FIG. 1. Principle and basic experimental setup for electrochemical promotion (NEMCA) studies utilizing an O^{2-} conducting solid electrolyte.

The effect of electrochemical promotion, or non-Faradaic electrochemical modification of catalytic activity (NEMCA effect) (11–22), has been discussed in the literature for more than 60 catalytic systems during the past few years. There have been several reviews (20–22) and a recent book (23). Its principle is shown schematically in Fig. 1. Potential or current application between the catalyst film and a second counter electrode deposited on the solid electrolyte leads to reversible and dramatic *in situ* modification of the chemisorptive and catalytic properties of the catalytic film. The induced catalytic rate increase is up to 150 times larger than the open-circuit rate value and up to 3×10^5 times larger than the rate of supply of ions onto the catalyst surface. Work in this area has been reviewed (20–24).

The origin of electrochemical promotion has been firmly established using a variety of surface science and electrochemical techniques, including work function measurements (15), X-ray photoelectron spectroscopy (XPS) (24, 25), ultraviolet photoelectron spectroscopy (UPS) (26), temperature-programmed desorption (TPD) (27, 28), scanning tunneling microscopy (STM) (29), cyclic voltammetry (27), and AC impedance spectroscopy (30, 31): electrochemical promotion is due to electrochemically controlled migration (backspillover) of ionic species ($O^{\delta-}$ in the case of O^{2-} conductors, $Na^{\delta+}$ in the case of Na^+ conductors, H^+ in the case of H^+ conductors) from the solid electrolyte onto the gas-exposed electrode surface.

These backspillover species form an overall neutral effective double layer on the gas-exposed electrode surface (22, 32, 33) and thus affect, acting as promoters or poisons, the chemisorptive and catalytic properties of the metal catalyst film.

The presence of this effective double layer on the catalyst surface not only induces electrochemical promotion (NEMCA) but also modifies the work function Φ of the catalyst surface according to the equation (15, 34)

$$\Delta\Phi = e\Delta U_{WR}, \qquad [1]$$

which is an important and relatively new equation in solid-state electrochemistry (13, 15, 32–37); ΔU_{WR} is the change in catalyst (working electrode, W) potential versus a reference (R) electrode induced either by changing the gaseous composition or by using a potentiostat. The adsorption- and spillover-modified work function Φ of the gas-exposed catalyst–electrode surface is, in general, different from the work function, Φ_O, of the *bare* metal surface. Positive ΔU_{WR} (i.e., O^{2-} supply *to* the catalyst) increases Φ by up to 1 eV (15, 32–37).

The complete oxidation of C_2H_4 on IrO_2, Pt, and Rh was chosen as a model reaction since its electrochemical promotion behavior on IrO_2 (12, 13), Pt (11), and Rh (14) porous films deposited on YSZ and on Pt porous films deposited on TiO_2 (38) is thoroughly studied (11–14) and also because the same reaction under identical experiment conditions has been studied on IrO_2–TiO_2 catalysts (13) and on Rh nanoparticles supported on various TiO_2 and YSZ supports (39).

The goal of the comparison was to examine which of the two types of catalyst activity promotion (electrochemical promotion or metal–support interactions) is stronger and in this way to gain information on the promoting mechanism of metal–support interactions, since the mechanism of electrochemical promotion (O^{2-} backspillover, concomitant (Eq. [1]) catalyst work function increase) is well established (21–33).

EXPERIMENTAL

The apparatus used for atmospheric pressure kinetic studies utilizing online gas chromatography (Perkin-Elmer 300B), mass spectrometry (Balzers QMG 311), and IR spectroscopy (Beckman 864 CO_2 analyzer) has been described previously (12, 14, 21, 38).

Reactants were Messer Griesheim-certified standards of C_2H_4 in He and O_2 in He. They could be further diluted in ultrapure (99.999%) He (L'Air Liquide).

Reactors. The atmospheric pressure single-chamber quartz reactor has a volume of 30 cm^3 and has been also described previously (12, 14, 21). It was used for the electrochemical promotion experiments of the IrO_2 and IrO_2–TiO_2 catalysts deposited on YSZ disks and of Pt films deposited on TiO_2. The closed-end YSZ tube reactor, also of volume 30 cm^3 and also described previously (14, 21, 38), has been used for the electrochemical promotion experiments of Rh films deposited on YSZ (38, 39). The equivalence of the single-chamber and closed-end tube CSTR reactors used routinely in electrochemical promotion studies has been discussed previously (20–22). The quartz tube CSTR reactor used for the kinetic studies on the dispersed nanoparticle Rh catalyst deposited on various powder supports has also been described previously (39). In all reactors used, the conversion of the reactants was kept below 20%.

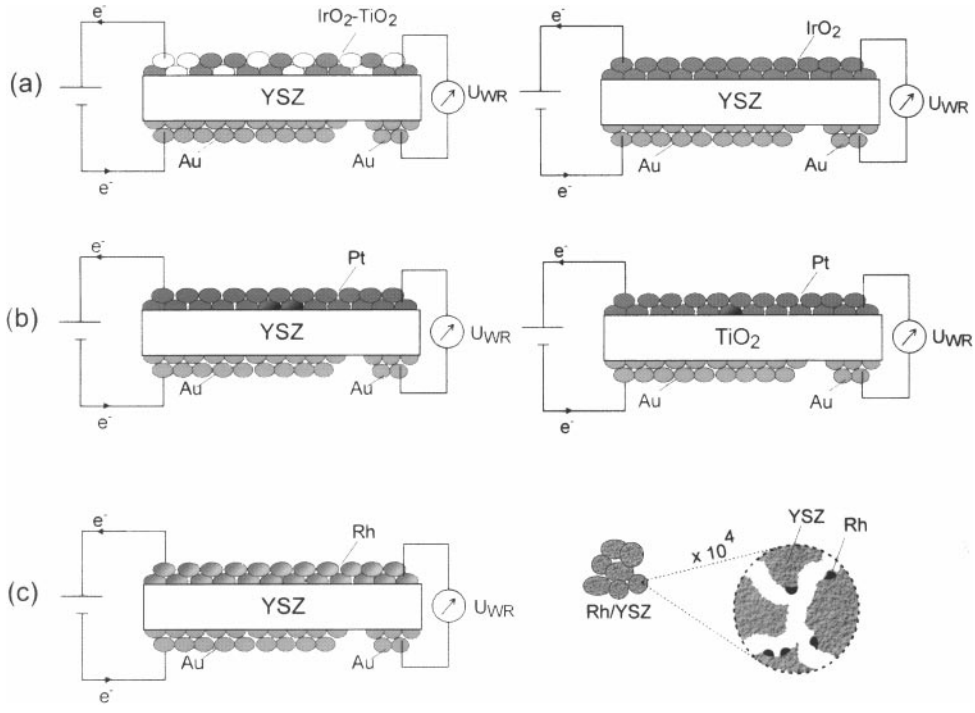

FIG. 2. Schematic of the experimental setup used to (a) induce electrochemical promotion (via YSZ) on IrO_2 and IrO_2–TiO_2 porous catalyst films, (b) compare the electrochemical promotion induced on Pt via YSZ and via TiO_2, and (c) compare the electrochemical promotion behavior induced by varying U_{WR} on a Rh porous catalyst film (left) and on a fully dispersed Rh catalyst supported on porous (80 m^2/g) YSZ support.

(IrO_2–TiO_2)/YSZ system. The IrO_2 and IrO_2–TiO_2 catalysts were deposited on YSZ via thermal decomposition of H_2IrCl_6 and $TiCl_3$ or $TiCl_4$ solutions (Fluka, Buchs). A micropipette was used to deposit 1-μL solution quantities on a 0.5-cm^2 YSZ surface followed by evaporation at 60°C, heating (20°C/min) in air to 550°C, and thermal treatment in air at 550°C for 10–60 min. The porous films were characterized by SEM and XPS. The latter confirmed that Ir and Ti are in the form of IrO_2 and TiO_2 and that the surface composition matches within 5% the bulk composition (13, 40, 41).

Rh/YSZ system. The porous Rh catalyst film was deposited on the inside bottom wall of the YSZ tube by application of a thin coating of Engelhard (Hanovia) A8826 Rh resinate, followed by drying and calcining in air, first at 400°C for 2 h and then at 850°C for 6 h. The thickness of the film was on the order of 10 μm, its superficial surface area was 2 cm^2, and its true surface area was 20 cm^2 (reactive oxygen uptake $N = 3.6 \times 10^{-8}$ g-atom O) determined by the isothermal titration technique (14, 21) using oxygen titration with CO at 350°C. Platinum counter and reference electrodes were deposited on the outer surface of the YSZ bottom wall using Engelhard Pt paste A-1121 followed by drying and calcination, first at 400°C for 2 h and then at 850°C for 6 h, as described elsewhere (14, 21).

Pt/YSZ and Pt/TiO_2 systems. The YSZ or TiO_2 (Merck Titanium(IV) Oxide Patinal, 11495) pellet was suspended in the quartz reactor by means of the Au wires attached to the three electrodes. The electrode arrangement is shown in Fig. 2. Prior to catalyst deposition, the TiO_2 tablet was sintered for 2 h at 1000°C. This should suffice for almost complete conversion of any anatase to rutile.

The Pt catalyst electrode was deposited on one side of the TiO_2 tablet by application of a thin coating of Engelhard Pt paste A-1121 followed by drying and calcination first (3°C/min) to 450°C for 1 h and then (2°C/min) to 830°C for 1 h. The Pt catalyst surface area (reactive oxygen uptake) was measured via surface titration of oxygen with C_2H_4 at 500°C and found to be 1.9×10^{-7} mol O.

Gold counter and reference electrodes were deposited on the opposite side of the TiO_2 tablet by using a Au paste prepared by mixing Au powder (Aldrich powder 99.9+, 32,658-5) in a slurry of polyvinyl acetate binder in ethyl acetate and following the same calcination procedure as with the Pt catalyst. A series of blank experiments showed that the TiO_2 tablet and the Au electrodes were inactive for C_2H_4 oxidation at temperatures up to 540°C.

In the same series of blank experiments (no Pt catalyst-electrode), currents up to 100 μA were applied between the two Au electrodes without any induction of catalytic activity for C_2H_4 oxidation. Consequently the observed catalytic phenomena can be safely attributed exclusively to the Pt catalyst only.

The experimental setup used previously (24, 38) to carry out the XPS investigations has been described previously

(24, 38). A 2-mm-thick TiO_2 slab (10×13 mm) with a Pt catalyst film, Pt reference electrode (deposited on the same side of the TiO_2 slab), and Ag counter electrode was mounted on a resistively heated Mo holder in an ultrahigh vacuum (UHV) chamber (base pressure 7×10^{-8} Pa), and the catalyst film (9×9 mm) was examined at temperatures of 25–520°C by XPS using a Leybold HS-12 analyzer operated at constant *DE* mode with 100-eV pass energy and a sampling area of 5×3 mm. Materials (TiO_2, Pt) and Pt catalyst deposition procedure were identical with the samples used for the atmospheric pressure kinetic study. Electron binding energies have been referenced to the metallic Pt $4f_{7/2}$ peak of the grounded catalyst at 71.1 eV, which always remains unchanged with no trace of nonmetallic (i.e., PtO_2) components.

Preparation and characterization of the dispersed Rh catalysts. The supported Rh catalysts were prepared by the method of incipient wetness impregnation of the supports with a solution of $Rh(NO_3)_2 \cdot 2H_2O$ (Alfa Products) of appropriate concentration to yield 0.05 or 0.5 wt% metal loadings. The following powder supports were used: SiO_2 (Altech Associates), TiO_2 (Degussa P25), ZrO_2 (8% Y_2O_3) (Zirconia Sales), and γ-Al_2O_3 (Akzo Chemicals). W^{6+}-doped TiO_2 was prepared following the procedure which has been described elsewhere (39). The dopant content was 0.45 at.%. The doped and undoped TiO_2 supports were thermally treated (5 h, 900°C) while the ZrO_2 (8% Y_2O_3) supports underwent thermal pretreatment at 1500°C during production. Details of the preparation procedure of the supported catalysts can be found elsewhere (39). Before any measurements, the catalysts were reduced in a quartz tube under He flow (80 cm^3/min) at 250°C for 1 h followed by H_2 flow (80 cm^3/min) at 400°C for 1 h.

Characterization of the catalysts was carried out in a BET apparatus (Accusorb 2100E, Micromeritics) with H_2 chemisorption at 298 K and N_2 and/or Ar physical adsorption at 77 K. Catalyst characterization details have been presented elsewhere (39).

Work function measurements. The work function Φ of metal (Pt, Au, Ag) catalyst films deposited on YSZ and doped TiO_2 supports was measured via a Kelvin probe (Besocke/DeltaPhi-Electronik, probe "S") with a 2.5-mm-diameter Au-grid vibrating condenser element placed ~500 μm from the metal electrode surface in the UHV system. As previously discussed (15, 21, 33), in the Kelvin probe "S" operation, the CPD signal is drawn from the vibrating Au grid so that the Kelvin probe lock-in amplifier circuit is entirely independent of the electrochemical circuit of the solid electrolyte sample. As recently shown (42, 43) in connection with Eq. [1] and with the concomitant definition of the absolute potential scale in solid-state electrochemistry (42, 43), such work function measurements of backspillover-modified metal electrodes deposited on solid electrolytes also yield the work function Φ of the solid electrolyte (42, 43). The same procedure has been used in the past for other types of solid electrolytes (44). Results presented here were obtained with Pt electrodes deposited on the various supports, but Ag electrodes also gave similar ($\pm$0.1 eV) results as expected on the basis of the absolute electrode potential theory (42, 43, 45, 46).

RESULTS AND DISCUSSION

(IrO_2–TiO_2)/YSZ System

Figure 3 shows a typical potentiostatic (constant imposed potential) electrochemical promotion transient of C_2H_4 oxidation on an IrO_2 catalyst film deposited on YSZ followed by galvanostatic (constant imposed current) interruption of the current ($I = 0$) after steady state has been achieved (12). Application of a positive overpotential ΔU_{WR} enhances reversibly the rate by more than a factor of 6. The rate enhancement ratio ρ defined from

$$\rho = r/r_o, \qquad [2]$$

where r_o is the open-circuit catalytic rate, is thus 7.6 for this experiment. The apparent Faradaic efficiency Λ is defined from

$$\Lambda = (r - r_o)/(I/2F), \qquad [3]$$

where I is the applied positive current, F is Faraday's constant, and $I/2F$ equals the rate of O^{2-} supply to the catalyst. In this experiment (Fig. 3), Λ equals 1760 (i.e., each O^{2-} supplied to the catalyst causes 1760 chemisorbed oxygen atoms to react with C_2H_4, forming CO_2 and H_2O). It is worth noting from Fig. 3 that the magnitude of the rate relaxation time constant is on the order of $2FN/I$, where N(in mol IrO_2) is the surface area of the IrO_2 catalyst film. This observation shows that indeed the electrochemical promotion behavior is due to the migration of O^{2-} on the gas-exposed electrode surface, since $2FN/I$ is the time required to form a monolayer of O^{2-} on a surface with N sites.

Figure 4 shows similar galvanostatic (constant imposed current) experiments obtained with IrO_2–TiO_2 samples with increasing TiO_2 mole fraction (13). The two phases (IrO_2 and TiO_2) are in intimate contact as shown by SEM (13). It is worth noting that with increasing TiO_2 content, the open-circuit rate ($t = 0$) increases substantially and at the same time the magnitude of ρ decreases drastically. Furthermore with increasing TiO_2 content, the rate tends to return very slowly toward its initial unpromoted value upon current interruption. This is a demonstration of "permanent NEMCA" first reported by Comninellis and coworkers (40, 41). But the most important point in Fig. 4 is that with increasing TiO_2 content in the IrO_2–TiO_2 catalyst, the NEMCA effect tends to disappear as shown by the decreasing ρ values.

This point is manifested clearly in Fig. 5, which shows the effect of increasing IrO_2 mole fraction X_{IrO_2} in the

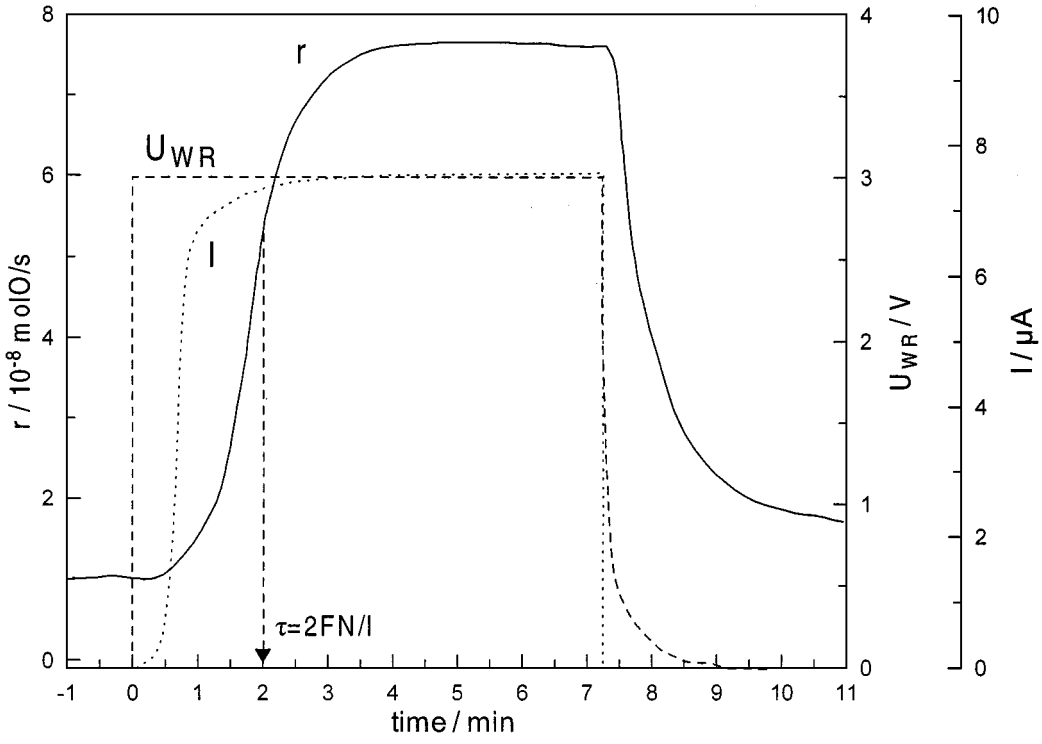

FIG. 3. Potentiostatic (constant potential U_{WR} imposition) catalytic rate (solid line), current (dotted line), and potential (dashed line) transients during C_2H_4 oxidation on a IrO_2 film deposited on YSZ followed by galvanostatic (constant current) interruption ($I = 0$); $T = 390^\circ$C, $p_{C_2H_4} = 0.26$ kPa, $p_{O_2} = 20$ kPa (based on Fig. 4.1 of Ref. (12)).

IrO_2–TiO_2 catalyst on the open circuit ($I = 0$) catalytic rate and on the electrochemically promoted ($I = 200\ \mu$A) catalytic rate. It is worth noting that:

1. Pure TiO_2 ($X_{IrO_2} = 0$) is catalytically inactive.
2. Pure IrO_2 ($X_{IrO_2} = 1$) has a moderate catalytic activity.
3. Addition of TiO_2 to the IrO_2 catalyst causes a pronounced enhancement in catalytic rate. Defining a promotional (metal–support interaction) rate enhancement ratio ρ_{MSI} by

$$\rho_{MSI} = r/r_u, \qquad [4]$$

where r_u is the (unpromoted) catalytic rate per unit mass of the active catalyst, one sees that ρ_{MSI} is up to 13 for $X_{IrO_2} = 0.5$.

4. Electrochemical promotion of the pure IrO_2 catalyst ($X_{IrO_2} = 1$) leads to a NEMCA rate enhancement ratio ρ up to 12.
5. Electrochemical promotion of the IrO_2–TiO_2 catalysts is negligible, with ρ values below 2.

Observations 3 to 5 very strongly suggest that the same type of promoting mechanism is operative for the TiO_2–IrO_2 catalyst and for the electrochemically promoted IrO_2 catalyst (Fig. 6). One may consider the IrO_2–TiO_2 metal–support interaction as a remote control mechanism (47, 48)

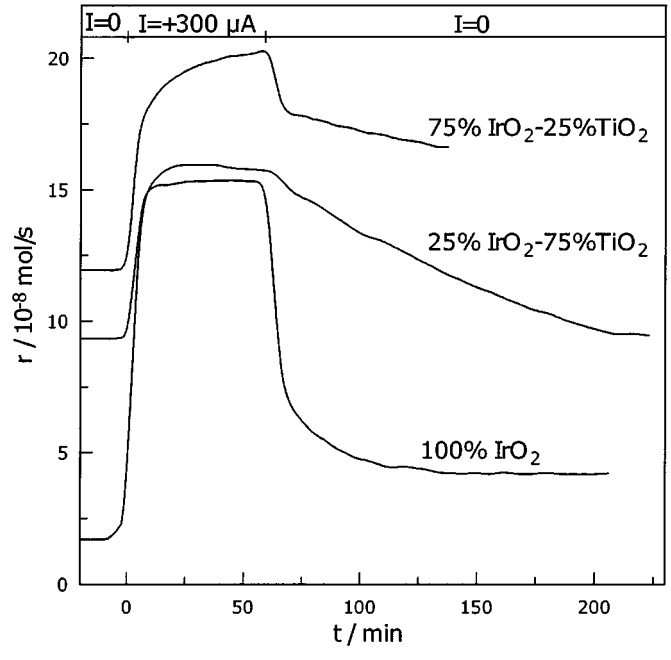

FIG. 4. Galvanostatic (constant current application) electrochemical promotion (NEMCA) transients during C_2H_4 oxidation on IrO_2–TiO_2 films deposited on YSZ; $T = 380^\circ$C, $p_{C_2H_4} = 0.15$ kPa, $p_{O_2} = 20$ kPa.

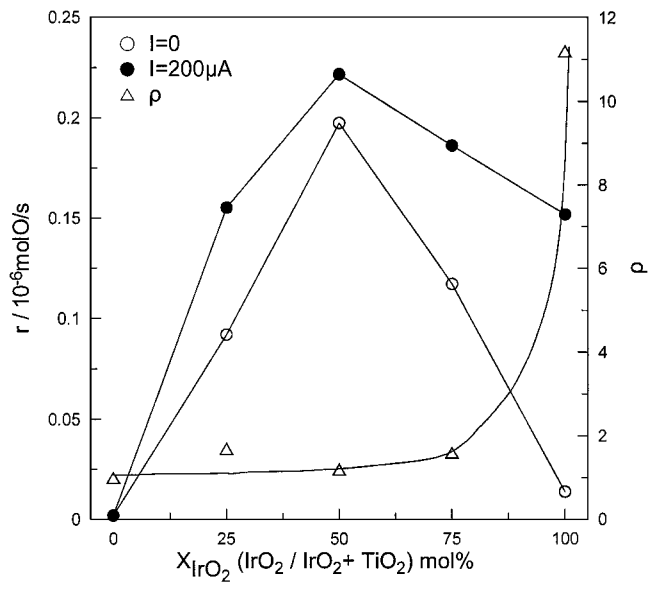

FIG. 5. Effect of the mole fraction, X_{IrO_2}, of IrO_2 in the IrO_2–TiO_2 catalyst film on the rate of C_2H_4 oxidation under open-circuit conditions (open circles) and under electrochemical promotion conditions (filled circles) via application of $I = 200$ μA, $T = 380°$C, $p_{C_2H_4} = 0.15$ kPa, $p_{O_2} =$ 20 kPa. Triangles indicate the corresponding rate enhancement ratio ρ value.

or as a "wireless" type NEMCA configuration (49, 50), where TiO_2 continuously provides promoting O^{2-} species to the IrO_2 catalyst surface and gaseous O_2 continuously replenishes spent O^{2-} in the TiO_2 (Fig. 6).

Electrochemical Promotion with YSZ and TiO_2

The complete equivalence between electrochemical promotion utilizing a solid electrolyte with purely ionic conductivity (YSZ) or a mixed ionic-electronic conductor (TiO_2) (Fig. 2b) has already been demonstrated for the case of C_2H_4 oxidation on Pt utilizing both kinetic measurements and XPS (38) (Figs. 7 and 8).

Thus Fig. 7 shows galvanostatic (constant current imposition) catalytic rate (NEMCA) transient obtained on Pt catalyst films (grain size ~ 1 μm) deposited on YSZ (21, 51) (Fig. 7a) and TiO_2 (38) (Fig. 7b) under similar (except for the temperature) experimental conditions. In particular, it is worth noting that the parameter $2FN/I$ (O^{2-} monolayer formation time) equals 810 s in Fig. 7a and 733 s in Fig. 7b.

In both cases, imposition of a positive current I (with a concomitant rate, $I/2F$, of supply of O^{2-} to the catalyst and an also concomitant increase in catalyst potential U_{WR}) causes a pronounced 25-fold increase in catalytic rate in Fig. 7a and a 22-fold increase in catalytic rate in Fig. 7b ($\rho = 26$ and $\rho = 23$, respectively).

The Faradaic efficiency Λ is 74×10^3 in Fig. 7a (YSZ) (21, 51) and 1.88×10^3 in Fig. 7b (38) (TiO_2), suggesting that only a fraction f ($\approx$2.5%) of the current I in TiO_2 is anionic (O^{2-}), the rest being electronic, in good agreement with the literature (38). This is nicely confirmed by comparing the time, τ, required for the rate increase to reach 63% of its steady-state value with the parameter $2FN/I$ (Fig. 7). In

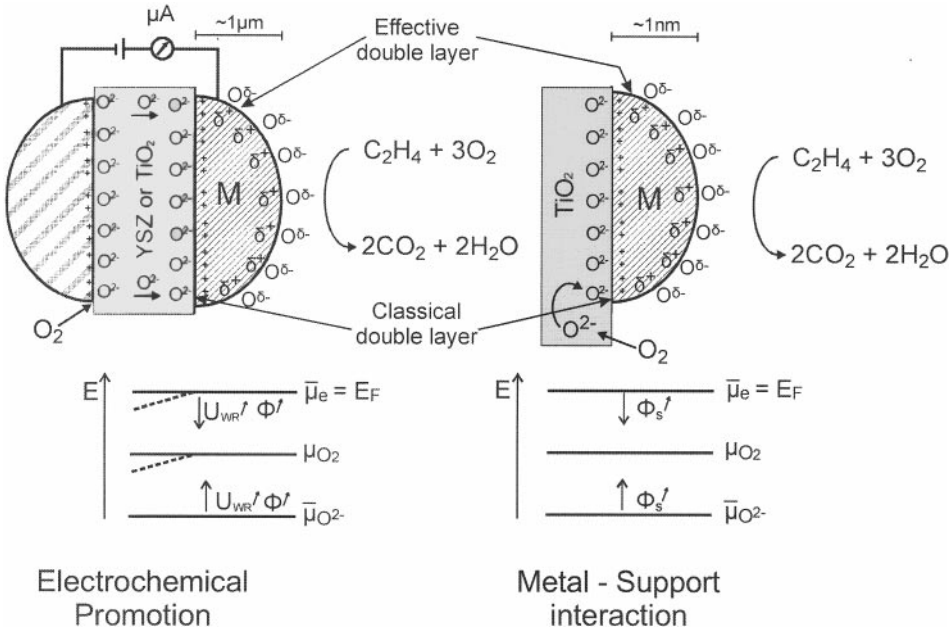

FIG. 6. Schematic of a metal grain ($\sim\mu$m) in a metal catalyst film deposited on YSZ or TiO_2 under electrochemical promotion conditions (left), of a metal nanoparticle ($\sim$nm) deposited on a porous TiO_2 support showing the locations of the classical double layers formed at the metal–support interface, and of the effective double layers formed at the metal–gas interface. The energy diagrams (bottom) indicate schematically the spatial constancy of the Fermi level E_F (or electrochemical potential $\bar{\mu}_e$) of electrons, of the chemical potential of oxygen, and of the electrochemical potential of O^{2-}. Note that under electrical bias application (left) $\bar{\mu}_{O^{2-}}$ remains spatially constant, but $\bar{\mu}_e$ and μ_{O_2} both bend in the solid electrolyte support (dashed lines). The Fermi level $\bar{\mu}_e$ of the metal can be affected by varying U_{WR} (left) or by varying via doping the Fermi level of the support (right).

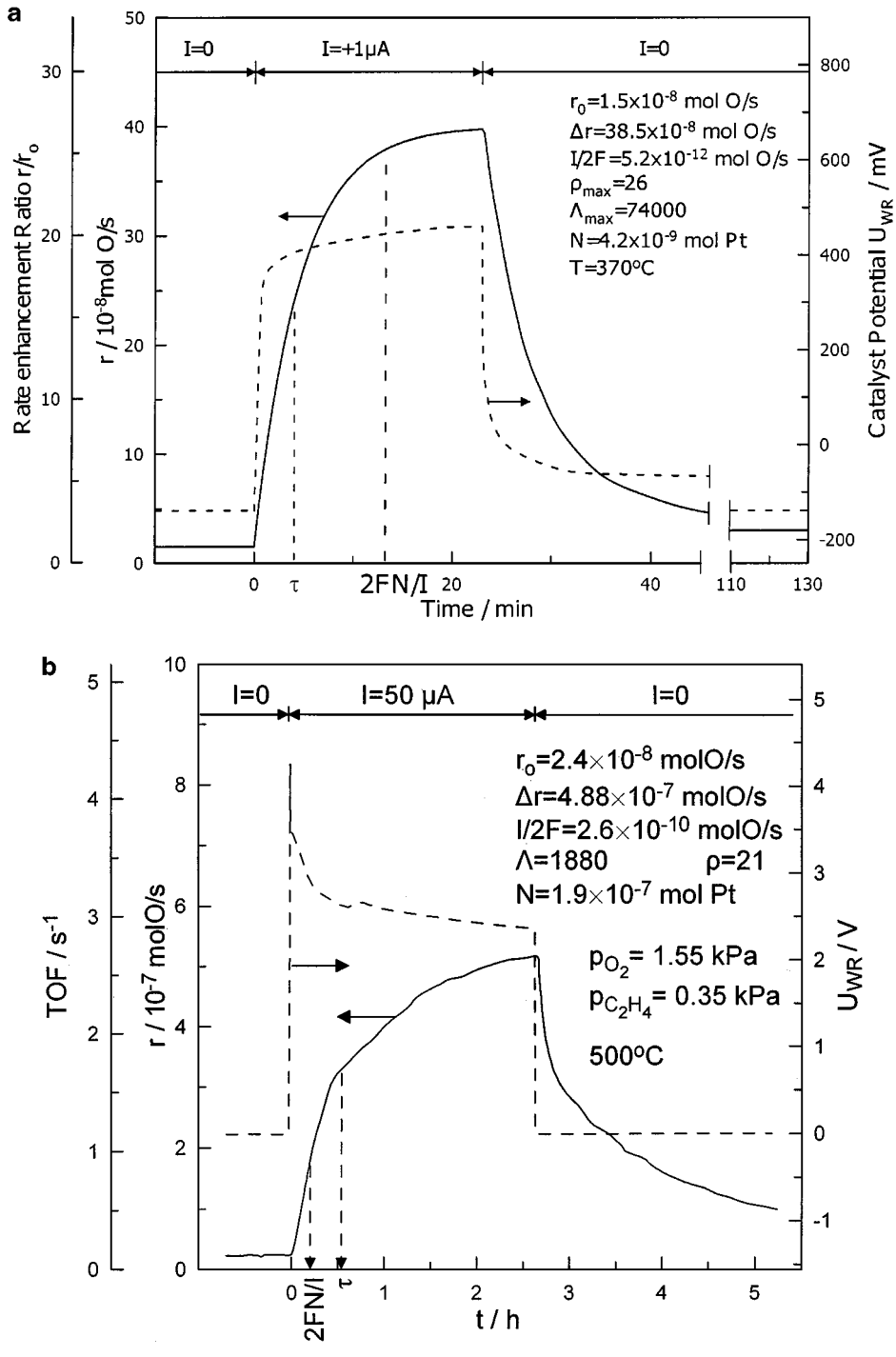

FIG. 7. Galvanostatic catalytic rate transients of C_2H_4 oxidation on Pt showing the equivalence of electrochemical promotion when (a) YSZ (21, 51) or (b) TiO_2 (38) is used as the Pt metal film support. See text for discussion.

the case of YSZ, τ is shorter than $2FN/I$ while in the case of TiO_2 τ is longer than $2FN/I$, again suggesting that only a fraction of the current I in TiO_2 is ionic. By comparing the ratio $\tau/(2FN/I)$ in both cases, one may conclude that $f \approx 0.05$, in qualitative agreement with the value estimated from the Faradaic efficiency, Λ, values.

Figures 8 and 9 confirm that O^{2-} backspillover from the support to the metal film surface is the promoting mechanism in the case of both YSZ (Fig. 8) and TiO_2 (Fig. 9). These figures show the O 1s spectrum of the Pt film deposited on YSZ and on TiO_2, first under open-circuit conditions (Figs. 8A and 9A) and then under positive current and potential application (Figs. 8B and 9B). Figures 8C and 9C show the difference spectra. In both cases, XPS clearly shows the presence of the O^{2-} double layer, even under open-circuit conditions (Figs. 8A and 9A). XPS also clearly

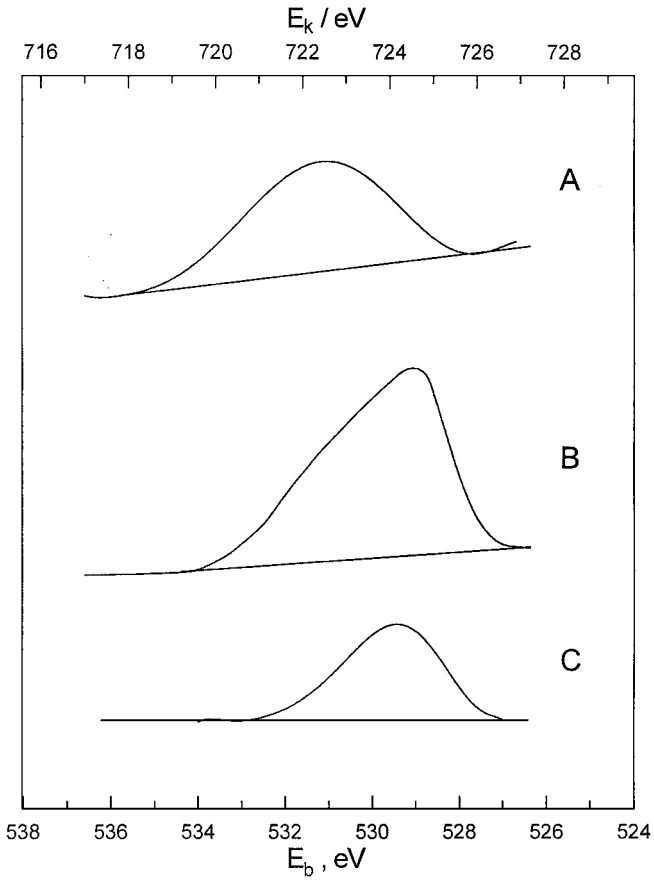

FIG. 8. XPS confirmation of $O^{\delta-}$ backspillover as the mechanism of electrochemical promotion on Pt films deposited on YSZ (24) (based on the data of Fig. 2a in Ref. (24)). (A) Open-circuit O1s spectrum. (B) O1s spectrum under anodic ($I = 40\ \mu$A, $\Delta U_{WR} = 1.2$ V) polarization. (C) Difference spectrum. $T = 400$°C. Reprinted, with permission, from ACS.

confirms the electrochemically controlled backspillover of O^{2-} from the YSZ or TiO_2 support onto the catalyst surface. Thus, as shown in Figs. 8B and 9B, upon anodic ($I > 0$, $\Delta U_{WR} > 0$) polarization, the O 1s spectrum grows significantly (by 60% in the case of YSZ (Fig. 8B) and by 15% in the case of TiO_2 (Fig. 9B)) with a concomitant shift to lower binding energies. This is also shown by the difference spectra (Figs. 8C and 9C), which correspond to the backspillover O species which has migrated on the Pt surface under the influence of the applied positive (anodic) potential. Note that the binding energy of the backspillover O species is in both cases near 529 eV, which confirms its strongly anionic (probably O^{2-}) state (24, 38).

Electrochemical Promotion of Rh Films and Support Effects on Dispersed Rh Catalysts

The kinetics of C_2H_4 oxidation on Rh were investigated on two types of model catalysts:

a. Polycrystalline porous Rh films deposited on YSZ at various potentiostatically imposed U_{WR} and thus Φ values (14, 39).

b. Fully dispersed nanoparticle Rh catalysts deposited on porous (~100 m^2/g) YSZ, TiO_2, doped TiO_2, γ-Al_2O_3, and SiO_2 supports (39).

Figure 10 shows the rate dependence on p_{O_2} for the dispersed Rh catalysts deposited on TiO_2, SiO_2, γ-Al_2O_3, YSZ (8 mol% Y_2O_3 in ZrO_2), and TiO_2 doped with 4 mol% WO_3. In all five cases, the Rh metal loading is 0.5 wt%.

The inset to Fig. 10 shows the rate dependence on p_{O_2} (at the same $p_{C_2H_4}$ and T) for the Rh *film* deposited on YSZ at various imposed potentials U_{WR}. The similarity between Fig. 10 and the inset to Fig. 10 is impressive and underlines the equivalence of metal–support interactions and electrochemical promotion: For low p_{O_2} values, the rate is first order in p_{O_2}, followed by a sharp decrease at a characteristic p_{O_2} value denoted by $p^*_{O_2}(U^*_{WR})$, which depends on the support (Fig. 10) or on the potential (inset to Fig. 10).

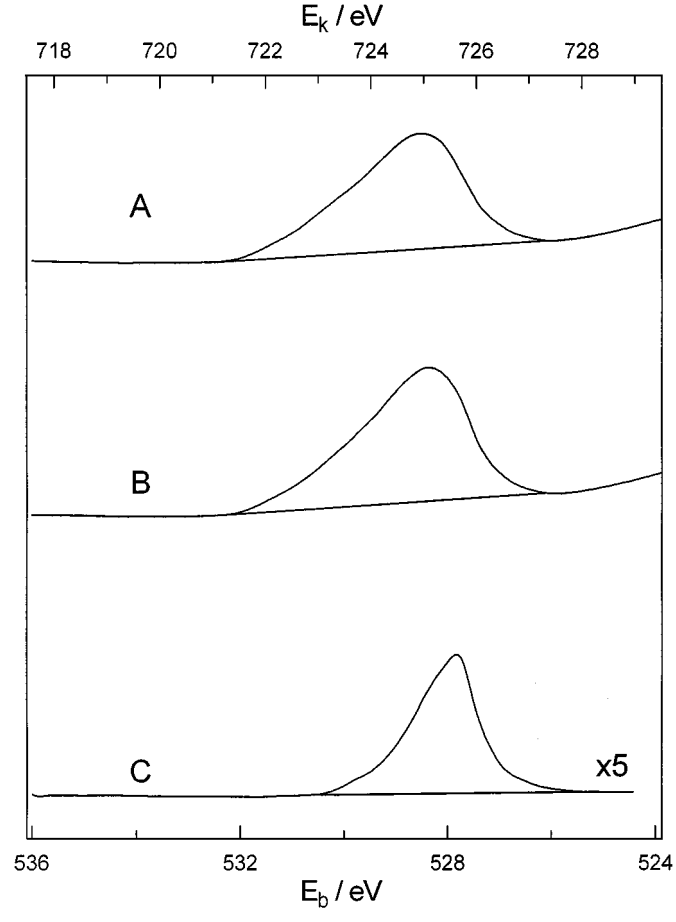

FIG. 9. XPS confirmation of $O^{\delta-}$ backspillover as the mechanism of electrochemical promotion on Pt films deposited on TiO_2 (38) (based on the data of Fig. 17a in Ref. (38)). (A) Open-circuit O1s spectrum. (B) O1s spectrum under anodic ($I = 100\ \mu$A, $\Delta U_{WR} > 0$) polarization. (C) Difference spectrum. $T = 500$°C.

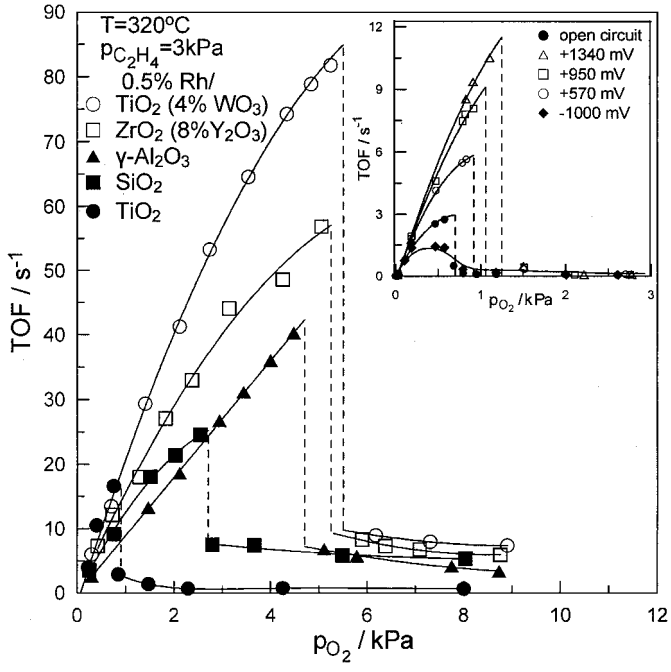

FIG. 10. Effect of p_{O_2} on the rate of C_2H_4 oxidation on Rh supported on five supports of increasing Φ. Catalyst loading 0.5 wt%. Inset: Electrochemical promotion of a Rh catalyst film deposited on YSZ. Effect of potentiostatically imposed catalyst potential U_{WR} on the rate and TOF dependence on p_{O_2} at fixed $p_{C_2H_4}$.

Thereafter the rate becomes very low and negative order in p_{O_2}. It has been shown that this sharp rate transition is due to the formation of a catalytically inactive surface Rh oxide (14, 39). As shown in Fig. 10 (inset), increasing U_{WR} and thus Φ cause a pronounced increase in $p^*_{O_2}$ and thus a dramatic rate increase at intermediate p_{O_2} values, with ρ values up to 100. Exactly the same behavior is obtained (Fig. 10) upon varying the dispersed catalyst support in the sequence TiO_2, SiO_2, γ-Al_2O_3, YSZ, and TiO_2 (4% WO_3). For intermediate p_{O_2} values, the metal–support interaction rate enhancement ratio ρ_{MSI} is up to 120 vs $\rho \approx 100$ for the electrochemically promoted system.

This destabilization of surface Rh oxide formation with increasing catalyst potential or work function has been shown to be due to strong lateral repulsive interactions of the backspillover O^{2-} species and normally chemisorbed oxygen (39), which causes a pronounced, up to 1 eV, decrease in the chemisorptive bond strength of normally chemisorbed O (27, 51).

Figure 11 is similar to Fig. 10, except for the Rh catalyst loading on the supports which is now a factor of 10 lower (i.e., 0.05 wt%). In this case, data with only four supports were taken, and the active Rh surface area, or dispersion, on the four supports was not exactly measured, so that the catalytic rate is expressed as moles of O per gram of catalyst per second and not as TOF (mol O consumed/(mol surface Rh) · s) as in Fig. 10 and other figures. Nevertheless the similarity with Fig. 10 is impressive as the same sequence of the supports is observed. Furthermore the similarity of Fig. 11 with the inset to Fig. 11 is again impressive. Note that the inset is the same as the inset to Fig. 10, because both insets refer to electrochemical promotion (NEMCA) of porous Rh films deposited on YSZ at the same temperature and gaseous composition as in Figs. 10 and 11.

Upon comparing Figs. 10 and 11, one concludes that the behavior is exactly the same and the sequence of the supports is again the same. As shown below, this sequence coincides with the sequence of increasing work function of the supports (33, 39, 42–44).

The electrochemical promotion data (insets to Figs. 10 and 11) show that for each imposed U^*_{WR} value there exists a corresponding p_{O_2} value, denoted already as $p^*_{O_2}(U^*_{WR})$, at which the sharp rate transition takes place, manifesting the formation of inactive surface Rh oxide (14, 39). As shown in Fig. 12 (filled circles), plotting eU^*_{WR} vs ln $p^*_{O_2}$ results in a straight line. This is quite reasonable considering that both the catalyst potential and ln p_{O_2} are linearly related to the chemical potential of adsorbed oxygen (21, 23). At the same time, referring now to the data of the supported catalysts (Figs. 10 and 11, not the insets), one can assign (via interpolation and extrapolation) to each of the observed rate transition, $p^*_{O_2}$, values a support (TiO_2–4% WO_3, YSZ, SiO_2, TiO_2). This has been done in Fig. 12 for each of the

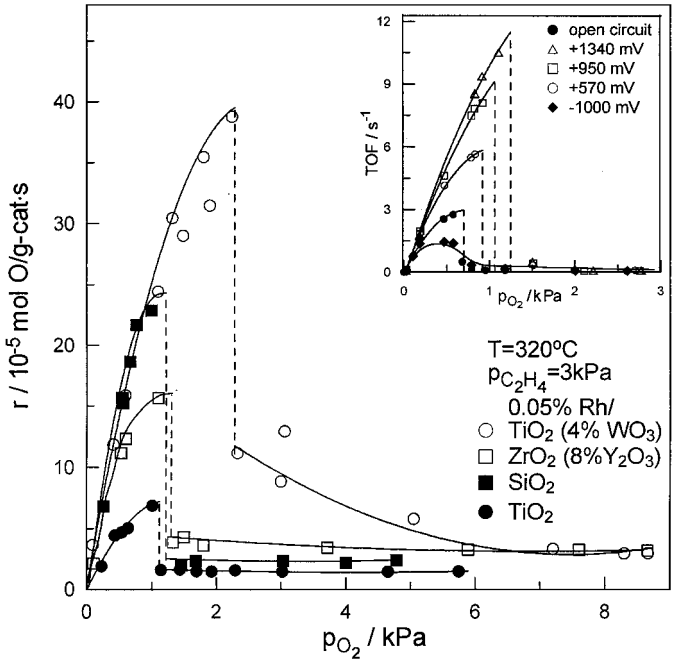

FIG. 11. Effect of p_{O_2} on the rate of C_2H_4 oxidation on Rh supported on four supports of increasing Φ. Catalyst loading 0.05 wt%. Inset: Electrochemical promotion of a Rh catalyst film deposited on YSZ. Effect of potentiostatically imposed catalyst potential U_{WR} on the rate and TOF dependence on p_{O_2} at fixed $p_{C_2H_4}$.

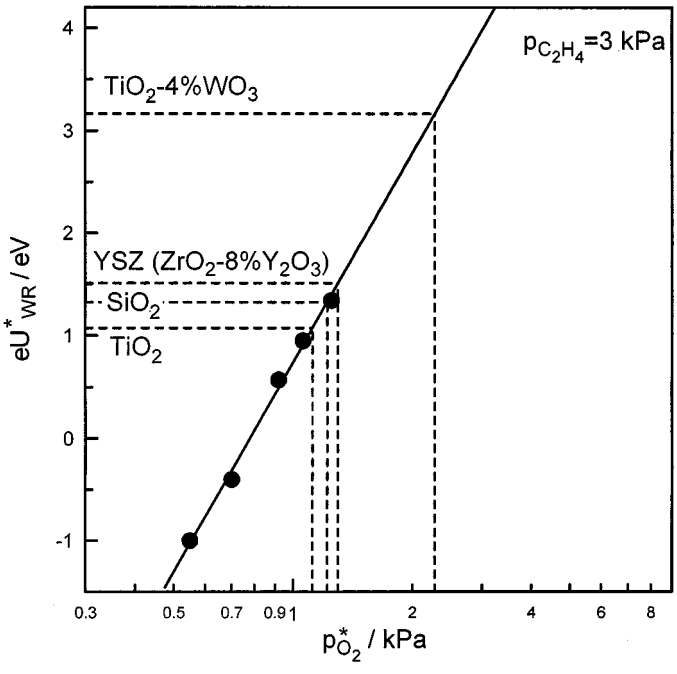

FIG. 12. (Filled circles) Interrelation between $p^*_{O_2}$ and potential U^*_{WR} at the sharp rate transition, during electrochemical promotion experiments of C_2H_4 oxidation on Rh films deposited on YSZ (Fig. 11, inset). Note the linearity between U^*_{WR} and ln $p^*_{O_2}$. (Dashed lines) Assignment (via interpolation and extrapolation in the $p^*_{O_2}$ scale) of equivalent U^*_{WR} potentials to the four supports of Fig. 11.

four supports of Fig. 11. Thus for each of these four supports we now have a corresponding equivalent U^*_{WR} value (Fig. 12). These values are plotted in Fig. 13 vs the actual work function Φ° measured via the Kelvin probe technique for the supports at $p_{O_2} = 1$ atm and $T = 400^\circ$C. The measuring principle utilizing a Kelvin probe and the pinning of the Fermi levels of support and metal electrodes in contact with it has been discussed elsewhere in conjunction with the absolute potential scale of solid-state electrochemistry (23, 42, 43, 45, 46).

The good qualitative agreement between eU^*_{WR} variation and Φ° variation shown in Fig. 13 for the various different supports used underlines again the common promotional mechanism of electrochemically promoted and metal–support interaction promoted metal catalysts.

The common underlying principle is shown in Fig. 6. The electrochemical potential of electrons $\bar{\mu}_e$ ($=E_F$, the Fermi level) in the metal catalyst is fixed at that of the Fermi level of the support (33, 42, 53). This is valid both for electrochemically promoted model catalysts (left) and for semiconducting or ion-conducting-supported metal nanoparticles (right).

The electrochemical potentials of electrons $\bar{\mu}_e$, oxygen ions $\bar{\mu}_{O^{2-}}$, and gaseous oxygen μ_{O_2} are related via the charge transfer equilibrium at the three metal–support–gas phase boundaries (20–22):

$$O_2(g) + 4e^-(M) \leftrightarrows 2O^{2-}(S). \qquad [5]$$

Here M is the metal catalyst and S is the support. This dictates

$$\bar{\mu}_{O^{2-}(S)} = 2\bar{\mu}_{e(M)} + (1/2)\mu_{O_2(g)}. \qquad [6]$$

However, to the extent that O^{2-} is mobile on the metal surface, one can also consider the equilibrium [5] being established also at the catalyst surface (in absence of fast desorption or fast catalytic reactions consuming the backspillover O^{2-} species) (24, 32, 33). In this case, one has

$$\bar{\mu}_{O^{2-}(M)} = 2\bar{\mu}_{e(M)} + (1/2)\mu_{O_2(g)}. \qquad [7]$$

Thus the difference $\bar{\mu}_{O^{2-}(S)} - \bar{\mu}_{O^{2-}(M)}$ is the thermodynamic driving force for O^{2-} backspillover from the support onto the catalyst surface (23, 32, 33) as proven by AC impedance spectroscopy (30, 31), STM (29), TPD (27, 28), and XPS (24, 25). It should be noted in Eqs. [6] and [7] that the Fermi level of the metal is also the Fermi level of the support.

In electrochemical promotion experiments (Fig. 6, left) one can vary $\bar{\mu}_{e(M)} = \bar{\mu}_{e(S)}$ by varying U_{WR} and thus also (Eq. [1]) Φ. In this way via Eq. [7] one can also vary the electrochemical potential and thus coverage of backspillover O^{2-} on the catalyst–electrode surface.

In dispersed metal–support systems (Fig. 6, right), one can vary $\bar{\mu}_{e(M)} = \bar{\mu}_{e(S)}$ by varying the support or by doping the support with aliovalent cations. This is known in

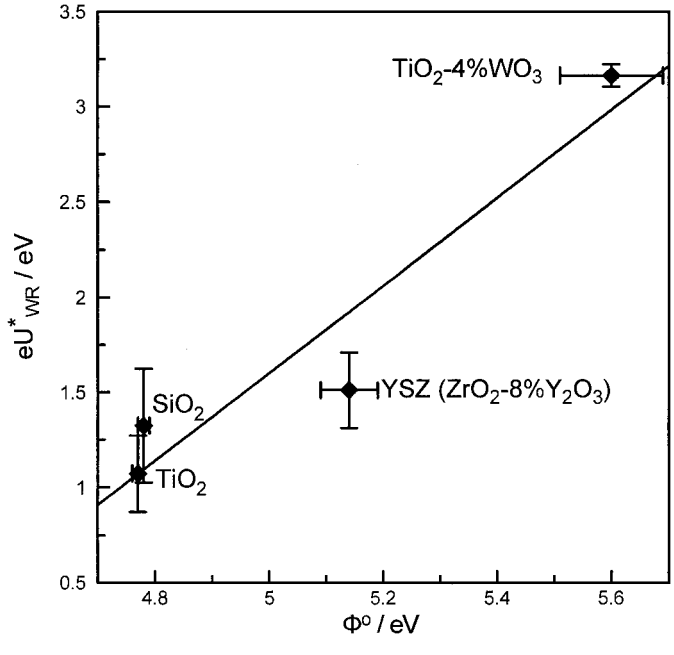

FIG. 13. Correlation between the equivalent potentials of the supports defined in Fig. 12 and the work function of the supports measured via the Kelvin probe technique in $p_{O_2} = 1$ atm at 400°C.

the literature as dopant-induced metal–support interactions (54–58). Thus one can again vary the electrochemical potential and thus the coverage of backspillover O^{2-} on the supported catalyst surface.

This simple model can account for the observed equivalence between electrochemical promotion and metal–support-induced promotional phenomena. In both cases, O^{2-} backspillover to the catalyst surface is the dominant promotional mechanism. A detailed mathematical model accounting for diffusion and reaction of the backspillover promoting species is presented elsewhere (23, 59). It should be noted that, according to the above equivalence, only electrophobic reactions (20–23) can be promoted by metal–support interactions on YSZ and TiO_2 (i.e., only reactions in which the rate increases with potential or work function (20–23)). This is nicely confirmed by the present results since C_2H_4 oxidation both on IrO_2 and on Rh is an electrophobic reaction ($\partial r/\partial U_{WR} > 0$) as also shown in Figs. 3–5 and 7. Detailed investigation of C_2H_4 oxidation on different metals and ion-conducting supports (60) has shown that it always exhibits electrophobic behavior under oxygen-rich conditions (23, 60).

CONCLUSIONS

The present results show the equivalence of electrochemical promotion and metal–support interactions on IrO_2 and Rh catalysts deposited on YSZ, TiO_2, and doped TiO_2 supports. Electrochemical promotion is an electrically controlled metal–support interaction. The corollary is that metal–support interactions on YSZ, TiO_2, and doped TiO_2 supports are similar to "wireless" NEMCA configurations tested already both on YSZ pellets (49, 61) and YSZ monoliths (50). The carrier continuously supplies promoting $O^{\delta-}$ species to the catalyst surface while spent O^{2-} in the support is continuously replenished by gaseous O_2.

ACKNOWLEDGMENTS

We thank BASF and Dupont for their financial support.

REFERENCES

1. Hegedus, L. L., *et al.*, *in* "Catalyst Design: Progress and Perspectives." Wiley, New York, 1987.
2. Bradford, M. C. J., and Vannice, M. A., *Catal. Today* **50**, 87 (1999).
3. Barton, D. G., Shtein, M., Wilson, R. D., Soled, S. L., and Iglesia, E., *J. Phys. Chem. B* **103**, 630 (1999).
4. Meitzner, G., and Iglesia, E., *Catal. Today* **53**, 433 (1999).
5. Beutel, T., Alekseev, O. S., Ryndin, Y. A., Likholobov, V. A., and Knözinger, H., *J. Catal.* **169**, 132 (1997).
6. Vaarkamp, M., Mojet, B. L., Kappers, M. J., Miller, J. T., and Köningsberger, D. C., *J. Phys. Chem.* **99**, 16067 (1995).
7. Wieckowski, A., Savinova, E., and Vayenas, C. G., *in* "Catalysis and Electrocatalysis at Nanoparticles." Dekker, New York, 2001.
8. Tauster, S. J., Fung, S. C., and Garten, R. L., *J. Am. Chem. Soc.* **100**, 170 (1978).
9. Haller, G. L., and Resasco, D. E., *Adv. Catal.* **36**, 173 (1989).
10. See, for example, Barteau, M. A., *Stud. Surf. Sci. Catal.* **130**, 105 (2000); Rossignol, S., Micheaud-Especel, C., and Duprez, D., *Stud. Surf. Sci. Catal.* **130**, 3327 (2000).
11. Vayenas, C. G., Bebelis, S., and Neophytides, S., *J. Phys. Chem.* **92**, 5083 (1988).
12. Varkaraki, E., Ph.D. thesis, Ecole Polytechnique Federal de Lausanne (EPFL), Lausanne, Switzerland, 1996.
13. Nicole, J., Ph.D. thesis, Ecole Polytechnique Federal de Lausanne (EPFL), Lausanne, Switzerland, 1999.
14. Pliangos, C., Yentekakis, I. V., Verykios, X. E., and Vayenas, C. G., *J. Catal.* **154**, 124 (1995).
15. Vayenas, C. G., Bebelis, S., and Ladas, S., *Nature* **343**, 625 (1990).
16. Pritchard, J., *Nature* **343**, 592 (1990).
17. Politova, T. I., Sobyanin, V. A., and Belyaev, V. D., *React. Kinet. Catal. Lett.* **41**, 321 (1990).
18. Harkness, I., and Lambert, R. M., *J. Catal.* **152**, 211 (1995).
19. Cavalca, C. A., and Haller, G. L., *J. Catal.* **177**, 389 (1998).
20. Vayenas, C. G. , and Neophytides, S., *in* "Electrochemical Activation of Catalysis: In Situ Controlled Promotion of Catalyst Surfaces," No. 12, p. 199. Royal Society of Chemistry, Cambridge, 1996.
21. Vayenas, C. G., Jaksic, M. M., Bebelis, S., and Neophytides, S. G., *in* "The Electrochemical Activation of Catalysis" (J. O. M. Bockris, B. E. Conway, and R. E. White, Eds.), No. 29, p. 57. Plenum Press, New York, 1996.
22. Vayenas, C. G., and Yentekakis, I. V., *in* "Electrochemical Modification of Catalytic Activity" (G. Ertl, H. Knözinger, and J. Weitcamp, Eds.), p. 1310. VCH Publishers, Weinheim, 1997.
23. Vayenas, C. G., Bebelis, S., Pliangos, C., Brosda, S., and Tsiplakides, D., *in* "The Electrochemical Activation of Catalysis." Plenum Press, New York, 2001.
24. Ladas, S., Kennou, S., Bebelis, S., and Vayenas, C. G., *J. Phys. Chem.* **97**, 8845 (1993).
25. Palermo, A., Tikhov, M. S., Filkin, N. C., Lambert, R. M., Yentekakis, I. V., and Vayenas, C. G., *Stud. Surf. Sci. Catal.* **101**, 513 (1996).
26. Zipprich, W., Wiemhöfer, H.-D., Vöhrer, U., and Göpel, W., *Ber. Bunsenges. Phys. Chem.* **99**, 1406 (1995).
27. Neophytides, S., and Vayenas, C. G., *J. Phys. Chem.* **99**, 17063 (1995).
28. Tsiplakides, D., and Vayenas, C. G., *J. Catal.* **185**, 237 (1999).
29. Makri, M., Vayenas, C. G., Bebelis, S., Besocke, K. H., and Cavalca, C., *Surf. Sci.* **369**, 351 (1996).
30. Kek, D., Mogensen, M., Pejovnik, S., *in* Proc. 3rd Intl. Symp. Electrocatal. (S. Hocevar *et al.*, Eds.), p. 257. Portoroz, Slovenia, 1999.
31. Frantzis, A. D., Bebelis, S., and Vayenas, C. G., *Solid State Ionics* **136–137**, 863 (2000).
32. Vayenas, C. G., *J. Electroanal. Chem.* **486**, 85 (2000).
33. Vayenas, C. G., and Tsiplakides, D., *Surf. Sci.* **467**, 23 (2000).
34. Ladas, S., Bebelis, S., and Vayenas, C. G., *Surf. Sci.* **251/252**, 1062 (1991).
35. Cavalca, C., Ph.D. thesis, Yale University, New Haven, CT, 1997.
36. Poppe, J., Shaak, A., Janek, J., and Imbihl, R., *Ber. Bunsenges. Phys. Chem.* **102**, 1019 (1998).
37. Poppe, J., Völkening, S., Schaak, A., Schütz, E., Janek, J., and Imbihl, R., *Phys. Chem. Chem. Phys.* **1**, 5241 (1999).
38. Pliangos, C., Yentekakis, I. V., Ladas, S., and Vayenas, C. G., *J. Catal.* **159**, 189 (1996).
39. Pliangos, C. A., Yentekakis, I. V., Papadakis, V. G., Vayenas, C. G., and Verykios, X. E., *Appl. Catal. B: Environ.* **14**, 161 (1997).
40. Nicole, J., and Comninellis, Ch., *J. Appl. Electrochem.* **28**, 223 (1998).
41. Foti, G., Wodiunig, S., and Comninellis, Ch., *Current Topics in Electrochemistry* **7**, 1 (2001).
42. Vayenas, C. G., and Tsiplakides, D., *Surf. Sci.* **467**, 23 (2000).
43. Tsiplakides, D., and Vayenas, C. G., *J. Electrochem. Soc.* **148**, E189 (2001).
44. Ukshe, E. A., *Soviet Electrochem.* **25**, 81 (1989).

45. Trasatti, S., *Electrochim. Acta* **36**, 1659 (1991).
46. Gileadi, E., Argade, S. D., and Bockris, J. O. M., *J. Phys. Chem.* **70**, 2044 (1966).
47. Delmon, B., and Froment, G. F., *Catal. Rev.—Sci. Eng.* **38**, 69 (1996).
48. Li, C., and Xiu, Q. (Eds.), "Spillover and Migration of Surface Species on Catalysts," Vol. 112. Elsevier, Amsterdam, 1997.
49. Marwood, M., and Vayenas, C. G., *J. Catal.* **168**, 538 (1997).
50. Wodiunig, S., Bokeloh, F., Nicole, J., and Comninellis, Ch., *Electrochem. Solid State Lett.* **2**, 281 (1999).
51. Bebelis, S., and Vayenas, C. G., *J. Catal.* **118**, 125 (1989).
52. Pacchioni, G., Illas, F., Neophytides, S., and Vayenas, C. G., *J. Phys. Chem.* **100**, 16653 (1996).
53. Riess, I., and Vayenas, C. G., Submitted for publication.
54. Akubuiro, E. C., and Verykios, X. E., *J. Catal.* **103**, 320 (1987); **113**, 106 (1988).
55. Karakitsou, K. E., and Verykios, X. E., *J. Phys. Chem.* **97**, 1184 (1993).
56. Ioannides, T., Verykios, X. E., Tsapatsis, M., and Economou, C., *J. Catal.* **145**, 497 (1994).
57. Zhang, Z., Kladi, A., and Verykios, X. E., *J. Phys. Chem.* **98**, 6804 (1994).
58. Ioannides, T., and Verykios, X. E., *J. Catal.* **161**, 560 (1996).
59. Vayenas, C. G., and Pitselis, G., *I&EC Res.* **40**, 000 (2001).
60. Bebelis, S., Makri, M., Buekenhoudt, A., Brosda, S., Petrolekas, P., Pliangos, C., and Vayenas, C. G., *Solid State Ionics* **129**, 33 (2000).
61. Cavalca, C. A., Larsen, G., Vayenas, C. G., and Haller, G., *J. Phys. Chem.* **97**, 6115 (1993).